Unveiling the interplay between magnetic fields and accretion in a young protocluster

MAX PLANCK INSTITUTE

Farideh. S. Tabatabaei[1], Elena Redaelli[1], Paola Caselli[1], Gabriel A. P. Franco[2], and Ana Duarte-Cabral[3]

[1]Max-Planck-Institut für extraterrestrische Physik, Munich - [2]Departamento de Física—ICEx—UFMG, Brazil - [3]Cardiff University, UK

Introduction:

Protostar formation depends on the balance between gravity, thermal pressure, external pressure, and magnetic field B. The role of the latter in the star formation process is still debated, and for this reason, it is important to study the structure of magnetic field lines in star-forming regions.

Source: Barnard 59:

The Pipe Nebula, which is located at a distance of d = 163 pc [1], is one of the closest known star-forming regions. B59 is located in the center of what resembles a hub-like clump with visually converging filaments [2]. A large fraction of the filaments around the B59 core is shaped by the outflows of the forming protocluster pushing the material rather than infalling filaments of gas [3]. The one clear exception is the filament to the NE of the clump, which is the object of this work (Figure 1).

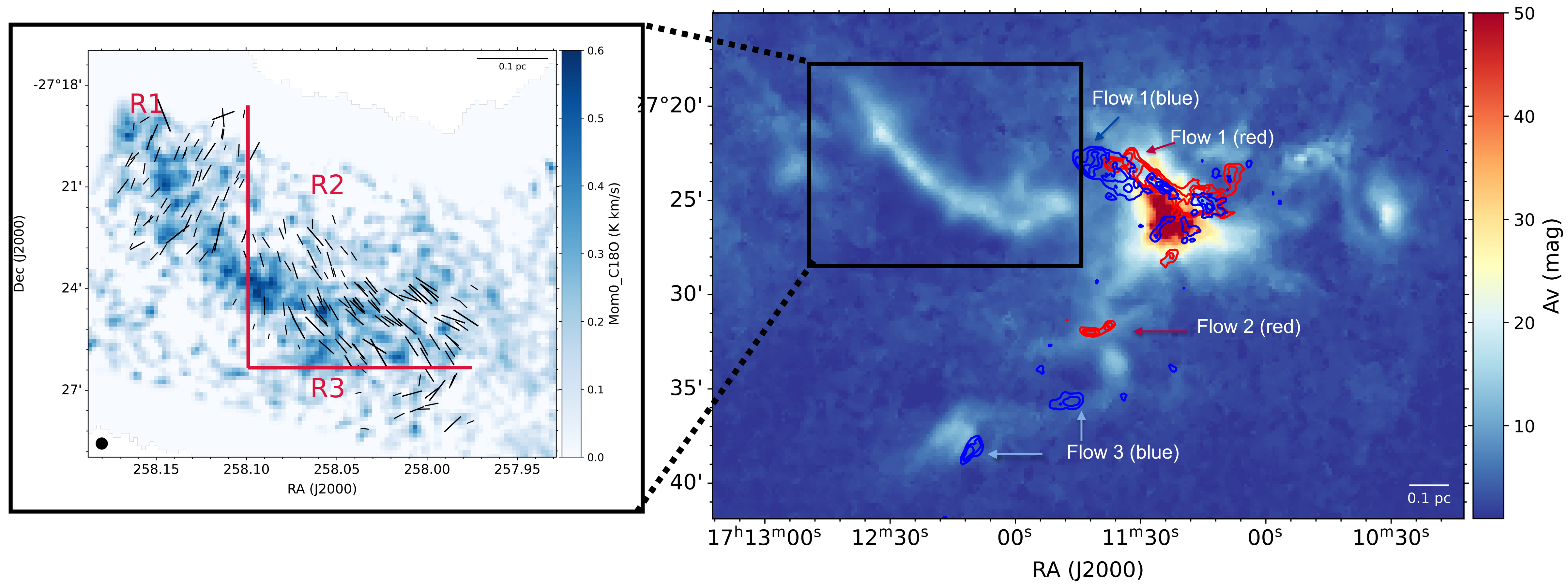

Figure 1: Right) Extinction map of B59 in color scale[4] and contours showing blue and red outflows. Left) The zooming is the moment 0 map of the $C^{18}O$ (3-2) line overlaid with the polarization vector from Pico dos Dias Observatory. R1, R2, and R3 regions divided the filament into 3 for the calculation of magnetic field strength.

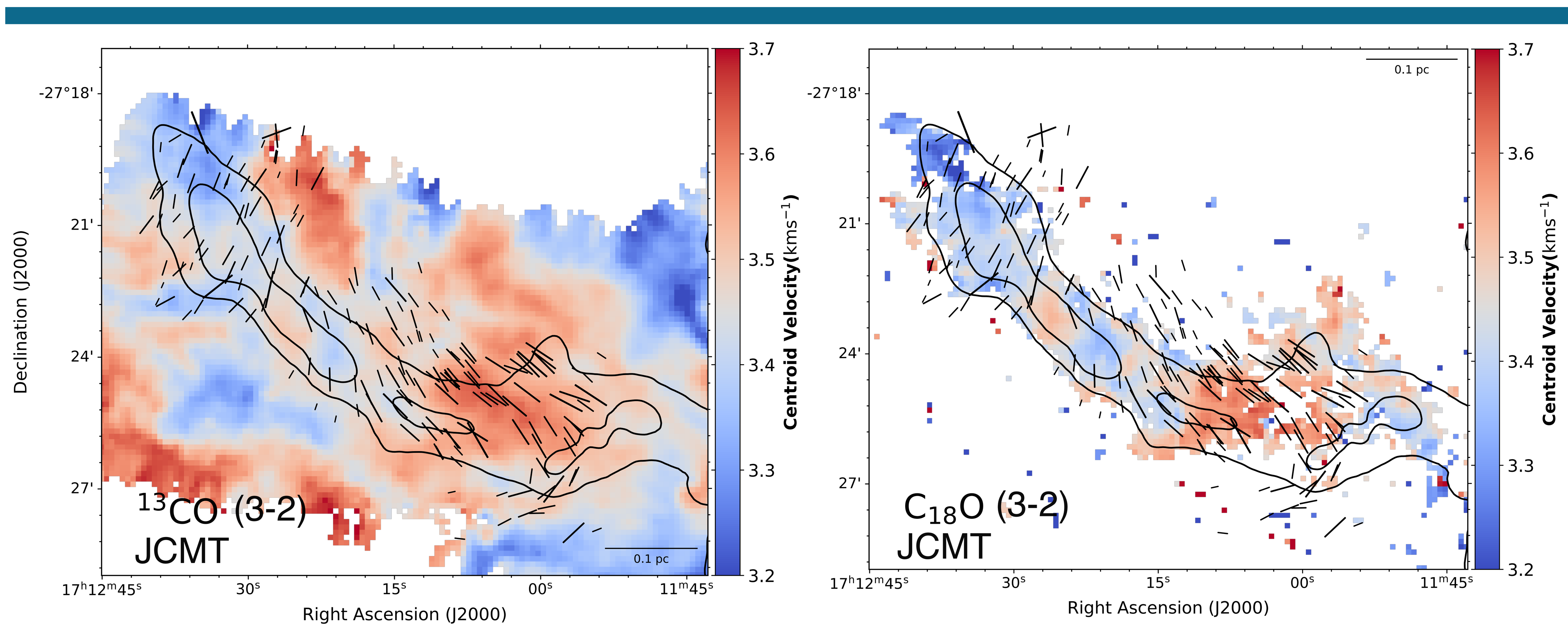

Figure 2: Centroid velocity maps of 13CO(3-2) and C18O (3-2) obtained from JCMT, and contours showing column density of H2 with levels: [4e+21,6e21]. Overlaid vectors are polarization in the NIR band.

Polarization and Kinematics:

The polarization data were collected with the telescopes at the observatory do Pico dos Dias (LNA/MCT, Brazil) in the near-infrared regime (black vectors in Figures 1 and 2).

The orientation of vectors shows two different directions, from parallel to the filament spine in the east region to perpendicular to it going towards the west. The change in the B-field where the filament connects to the hub suggests a coupled evolution of the B-field and the filaments. The reorganization of the B-field along the filament could be caused by local velocity flows of matter in-falling towards the hub, where the B-field is dragged by gravity and flows along the filaments (Figure 2, Centroid velocity of 13CO and C18O).

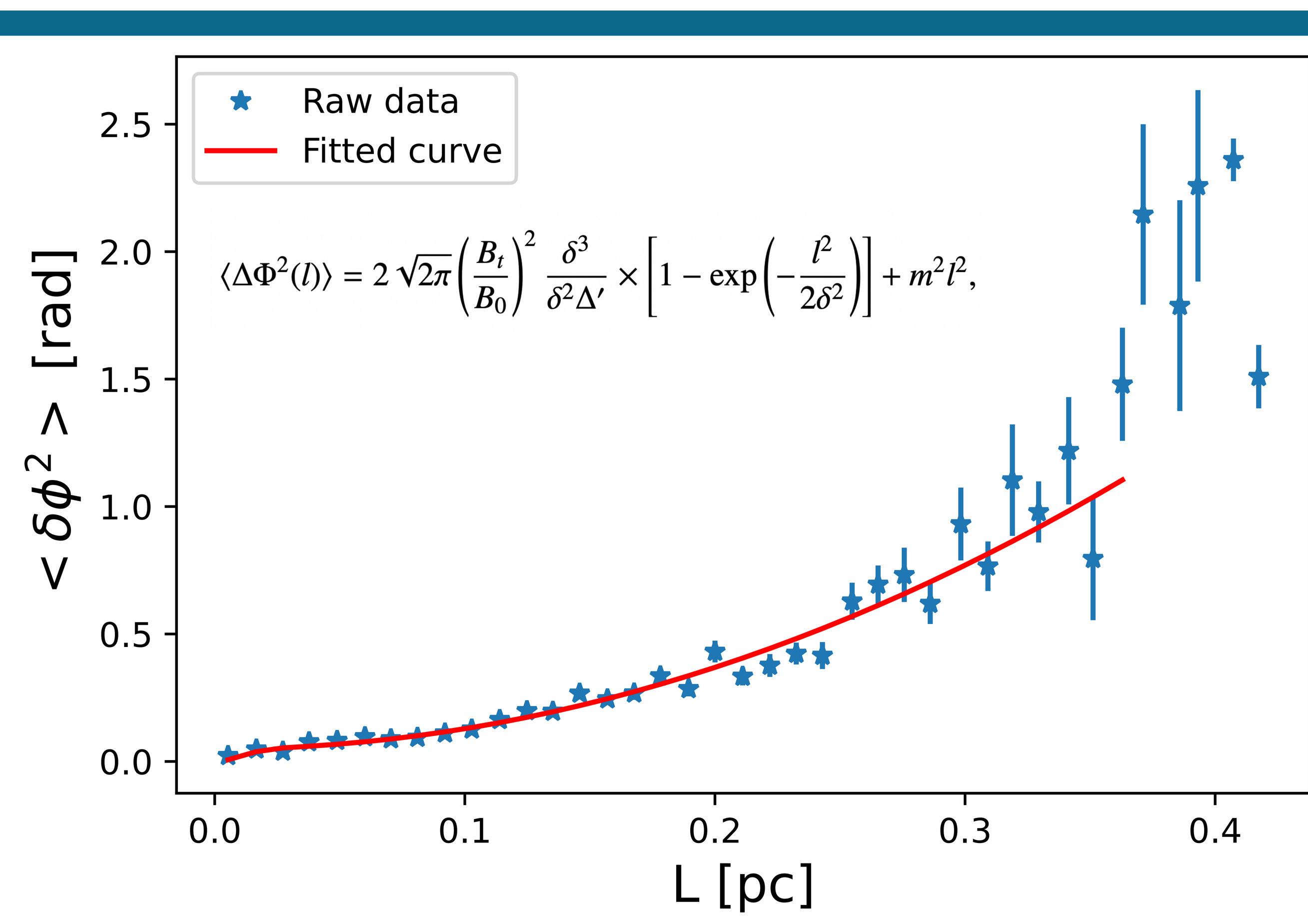

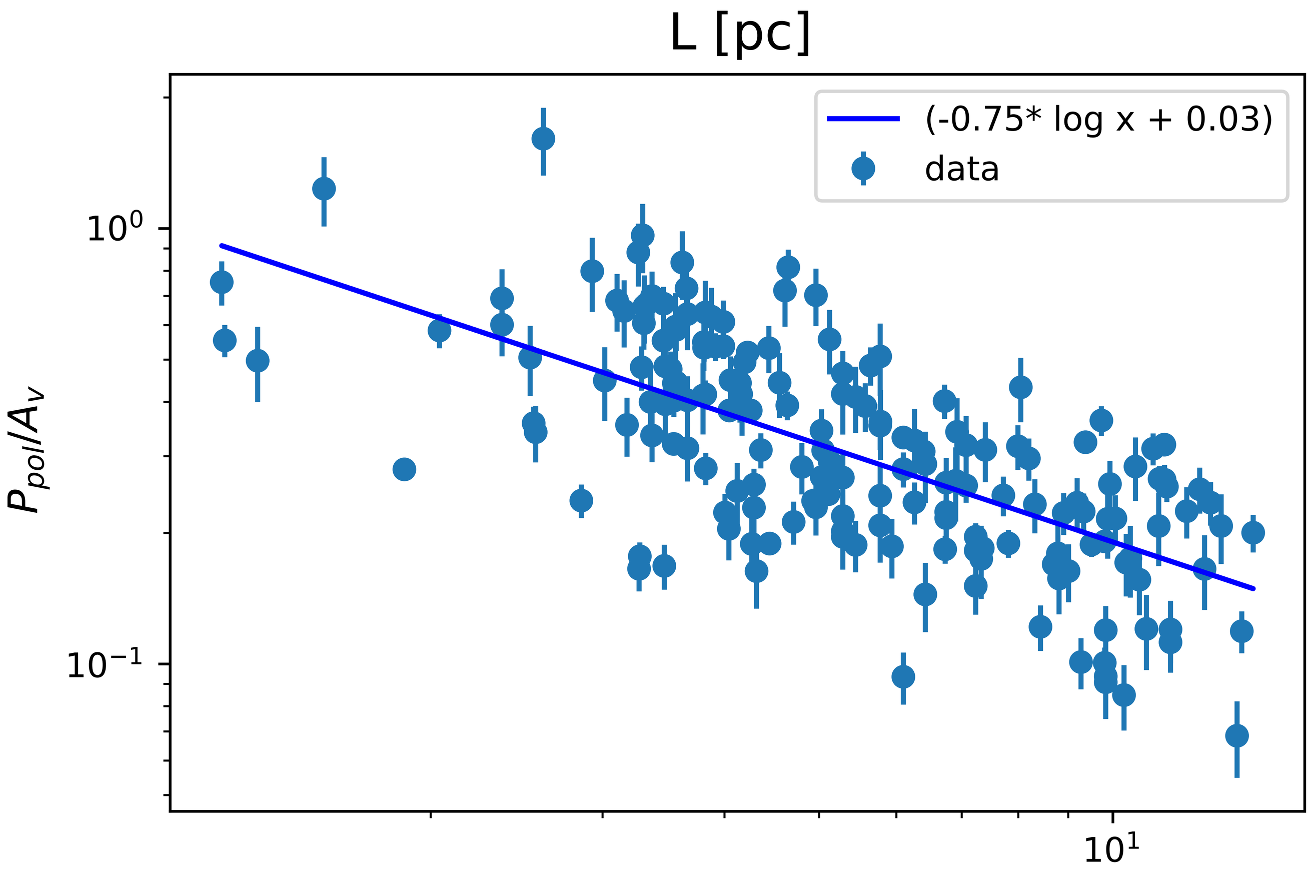

Polarization analysis:

- With the use of DCF and HH09 methods [5], [6], and [7], we calculate the autocorrelation function of the position angles $\Delta\Phi$. This refers to the variation in the angle between every pair of vectors divided by a distance L (Figure 3, only region R2). We plot the angular dispersion function for each region shown in Figure 1 and, with the best-fit parameters, calculate the magnetic field strength on the plane-of-sky (Table 1, B_{pos} parameter).
- The polarization efficiency versus visual extinction plot shows depolarisation at high column densities (Figure 4). At higher visual extinction, less radiation penetrates into the cloud; then the dust grains are less aligned. We find α = 0.75 the slope of relation $P_{pol}/A_{\mathrm{v}} \sim A_{\mathrm{v}}^{-\alpha}$ which is consistence with RAT theory and previous studies.
- A parameter to characterize the importance of the field in the dynamics and balance of the cloud is the mass-to-flux ratio normalized to its critical value. Our analysis shows that the ratio is lower than the critical value, so the cloud is subcritical, which means the magnetic field stabilizes gravity (Table 1, λ parameter).

Top) Figure 3: Angular dispersion function with respect to the distance L; the measurement uncertainties are shown as error bars. The best fit to the data points is in the red curve.

Botton) Figure 4: Mean polarization versus visual extinction. The solid line is the best fit for the dataset. The best-fit equation is shown in the top right corner.

Table 1: Obtained Physical Parameters for the Three Regions in the filament

Regions	B_t/B_0	m [rad/pc]	$B_{\rm pos}$ [μG]	$B^*_{\rm pos}$ [μG]	λ
R1	0.98 ± 0.02	1.7 ± 0.1	59.4 ± 1.1	41.8 ± 0.6	0.6 ± 0.1
R2	0.53 ± 0.01	2.83 ± 0.04	80.2 ± 0.9	48.5 ± 0.5	0.50 ± 0.08
R3	1.3 ± 0.2	11.6 ± 0.9	52.4 ± 6	39.2 ± 3	0.8 ± 0.1

References: [1] Dzib, S. A., Loinard, L., Ortiz-Leon, G. N., et al. 2018, ApJ, 867, 151; [2] Peretto N. et al., 2014, A&A, 561, A83; [3] Duarte-Cabral, A., Chrysostomou, A., Peretto, N., et al. 2012, A&A, 543, A140; [4] Román-Zúñiga, C. G., Frau, P., Girart, J. M., & Alves, J. F. 2012, ApJ, 747, 149; [5] Chandrasekhar, S., & Fermi, E. 1953, ApJ, 118, 116; [6] Hildebrand, R. H., Kirby, L., Dotson, J. L., Houde, M., & Vaillancourt, J. E. 2009, ApJ, 696, 567; [7] Houde, M., Vaillancourt, J. E., Hildebrand, R. H., Chitsazzadeh, S., & Kirby, L. 2009, ApJ, 706, 1504

For further information please contact: farideht@mpe.mpg.de